Flux of carbonate melt from deeply subducted pelitic sediments: Geophysical and geochemical implications for the source of Central American volcanic arc

Kyusei Tsuno,[1] Rajdeep Dasgupta,[1] Lisa Danielson,[2] and Kevin Righter[3]

Received 5 June 2012; revised 6 July 2012; accepted 11 July 2012; published 24 August 2012.

[1] We determined the fluid-present and fluid-absent near-solidus melting of an Al-poor carbonated pelite at 3–7 GPa, to constrain the possible influence of sediment melt in subduction zones. Hydrous silicate melt is produced at the solidi at 3–4 GPa whereas Na-K-rich carbonatite is produced at the solidi at ≥5 GPa for both starting compositions. At ≥5 GPa and 1050°C, immiscible carbonate and silicate melts appear with carbonate melt forming isolated pockets embedded in silicate melt. Application of our data to Nicaraguan slab suggests that sediment melting may not occur at sub-arc depth (∼170 km) but carbonatite production can occur atop slab or by diapiric rise of carbonated-silicate mélange zone to the mantle wedge at ∼200–250 km depth. Flux of carbonatite to shallower arc-source can explain the geochemistry of Nicaraguan primary magma (low SiO_2 and high CaO, Ba/La). Comparison of carbonate-silicate melt immiscibility field with mantle wedge thermal structure suggests that carbonatite might temporally be trapped in viscous silicate melt, and contribute to seismic low-velocity zone at deep mantle wedge of Nicaragua. **Citation:** Tsuno, K., R. Dasgupta, L. Danielson, and K. Righter (2012), Flux of carbonate melt from deeply subducted pelitic sediments: Geophysical and geochemical implications for the source of Central American volcanic arc, *Geophys. Res. Lett.*, *39*, L16307, doi:10.1029/2012GL052606.

1. Introduction

[2] The mass exchange and chemical differentiation process in subduction zones are promoted by the liberation of fluids and/or fluid-induced partial melts from the slab, which cause arc volcanism and interplate earthquakes and affect mantle wedge dynamics, plate tectonics, and long-term volatile transfer to the exosphere. Although the arc flux of both CO_2 and H_2O are shown to originate from the subducting slab lithologies [e.g., *Snyder et al.*, 2001; *Shaw et al.*, 2003; *de Leeuw et al.*, 2007; *van Keken et al.*, 2011], slab-mantle transfer of the former is a poorly understood process. Devolatilization reactions of the slab lithologies, as constrained by free energy minimization calculation under subsolidus conditions suggest that while most water is quantitatively released to the shallow mantle wedge, mineral carbonates subduct past sub-arc depth with a limited solution of CO_2 in slab-derived hydrous melts or fluids [e.g., *Kerrick and Connolly*, 2001a, 2001b; *Tsuno and Dasgupta*, 2012]. In other words, dehydration melting releases a fluid high in H_2O/CO_2 ratio. However, the possible role of melting of carbonate-bearing ocean-floor sediments remains a less explored process.

[3] Considering efficient dehydration of subducting sediment at forearc depths, it is important to constrain the melting of subducting carbonated pelite under water-poor conditions. Because the solidi of carbonated pelites [*Thomsen and Schmidt*, 2008; *Tsuno and Dasgupta*, 2011, 2012] are the lowest among all the carbonate-bearing slab lithologies [*Yaxley and Brey*, 2004; *Dasgupta et al.*, 2004, 2005; *Gerbode and Dasgupta*, 2010; *Dasgupta and Hirschmann*, 2010; *Kiseeva et al.*, 2012] and ocean-floor sediments subduct along the hottest path experienced by any subducting lithologies [e.g., *Syracuse et al.*, 2010], partial melt from sedimentary material has the best prospect of carrying CO_2 to the arc source. However, hydrous silicate melting of carbonated sediments occurs at temperatures higher than the estimated slab-top temperatures at ∼100 km depth [*Syracuse et al.*, 2010; *Cooper et al.*, 2012] and higher pressure experimental data on the partial melting of carbonated sediment are limited to an Al-rich bulk composition relevant only for Lesser Antilles subduction zone [*Thomsen and Schmidt*, 2008; *Grassi and Schmidt*, 2011a]. While carbonate breakdown in Al-rich sediment even at depths up to 200 km does not occur along any reasonable subduction *P-T* paths, whether carbonate melting occurs for alumina-poor pelite relevant for the subduction zones at Central America, Sunda, and Vanuatu (auxiliary material, Table S1 in Text S1) remains unknown.[1] In particular, relatively young and steeply dipping Cocos plate achieves the highest slab-surface temperature beneath the volcanic front among all the subduction zones that contain significant carbonate fraction in their downgoing sediment budget; therefore, the possibility of sedimentary carbonate melting at deep sub-arc depths merits consideration.

[4] Here we constrain melting phase relations of an alumina-poor carbonated pelite similar to the sediments subducting in East Sunda and Vanuatu and in particular what might be encountered in the deep mélange zone between carbonate and hemipelagic unit of Central American subduction zone. The experiments were conducted to pressures similar to the depth of the steeply dipping Cocos plate below Nicaraguan arc front. We present the relative depletion of bulk sediment H_2O and CO_2 as a function of depth and

[1]Department of Earth Science, Rice University, Houston, Texas, USA.
[2]ESCG, Houston, Texas, USA.
[3]NASA Johnson Space Center, Houston, Texas, USA.

Corresponding author: K. Tsuno, Department of Earth Science, Rice University, 6100 Main St., MS 126, Houston, TX 77005, USA. (kyusei.tsuno@rice.edu)

0094-8276/12/2012GL052606

[1]Auxiliary materials are available in the HTML. doi:10.1029/2012GL052606.

temperature and discuss such data in the light of geochemical variability of Central American arc magmas. We also argue that carbonated melting of hemipelagic sediment may influence the geophysical properties of the Central American mantle wedge. Our data have implications for CO_2 cycling in deep subduction zones in general and that of Nicaragua in particular.

2. Experimental Procedure

[5] Relative to the sediments that enter the trenches of Central America, Sunda and Vanuatu (DSDP site 495 [*Plank and Langmuir*, 1998]), the bulk starting compositions studied here (HPLC3 and HPLC4; Table S1 in Text S1) are poorer in SiO_2, as expected for pelitic sediments from which some finite fraction of siliceous hydrous fluid has been extracted during subduction at shallower depths. HPLC3 and HPLC4 include 5 wt.% CO_2 and 1 wt.% H_2O, and 5 wt.% CO_2 and 0.5 wt.% H_2O, respectively. The K_2O/H_2O molar ratios are 0.4 for HPLC3 and 0.8 for HPLC4, compared to ~0.5 for K-mica; this indicates fluid-present and fluid-absent subsolidus conditions for HPLC3 and HPLC4, respectively. Both starting materials are prepared by mixing reagent grade and natural oxides, hydroxides, and carbonates following the procedures detailed in *Tsuno and Dasgupta* [2012].

[6] High-pressure experiments at 3 GPa and 800–1150°C were performed using end-loaded piston cylinder (PC) and half-inch $BaCO_3$ cell assembly at Rice University, following the pressure calibration of *Tsuno and Dasgupta* [2011]. Experiments at 4–7 GPa and 900–1100°C were performed using a Walker-type multi-anvil (MA) apparatus at NASA-JSC (auxiliary material). The starting mix was enclosed in 2 mm outer diameter Au capsule for all the experiments, with run duration varying from 53 to 249 h. The absence of graphite and presence of carbonate in our experiments suggest fO_2 > EMOG buffer at all pressures. Recovered experiments were ground longitudinally and polished dry using diamond powders on soft nylon and velvet cloths to aid preservation of delicate carbonates. Table 1 reports the obtained phases identified using an FEI Quanta 400 FEG-SEM at Rice University and estimated phase proportions obtained by mass balance calculations. Mineral and melt compositions were obtained using WDS and EDS method using a Cameca SX-100 electron microprobe at NASA-JSC and FEG-SEM, respectively and those for 5 and 7 GPa experiments are reported in Table S2 in Text S1. Approach to equilibrium was verified by comparing the estimated temperatures based on garnet-cpx [*Krogh Ravna*, 2000] and garnet-phengite [*Green and Hellman*, 1982] Fe^{2+}-Mg K_D and garnet-carbonate Ca-Mg K_D [*Yaxley and Brey*, 2004] with the nominal experimental temperatures, which yielded average difference of ~58°C.

3. Results: Phase Assemblage and Texture

[7] The subsolidus phases include cpx, garnet, coesite, rutile, phengite, and $calcite_{ss}$ for both HPLC3 and HPLC4 at 3–5 GPa (Figure 1 and Table 1). The subsolidus assemblage for HPLC3 and HPLC4 also includes water-vapor and potassium feldspar (Figure 1a), respectively with the latter indicating fluid absent conditions. Solidi were bracketed using textural criteria. While above the solidus, small-volume melt occupied triple junctions and edges of residual minerals (Figure 1b), no such phase was present below the solidus (Figure 1a). Melt-free porosity and spherical voids in melt pool were interpreted as the presence of an equilibrium fluid phase. All the experiments across the solidus for HPLC3 were fluid-present whereas fluid phase in HPLC4 appeared only after complete breakdown of crystalline carbonate. We bracketed the solidus temperatures of 800–850°C at 3 GPa, <900°C at 4 GPa, 900–950°C at 5 GPa, and <1000°C at 7 GPa for HPLC3, and of 850–900°C at 3 GPa and 900–950°C at 5 GPa for HPLC4 (Figures 1c and 1d and Table 1). The near-solidus melts at 3–4 GPa for HPLC3 and at 3 GPa for HPLC4 are hydrous silicate, and those at 5–7 GPa are carbonatitic for both starting materials (Figure 1b). The complete breakdown of phengite was noted at 850–900°C at 3 GPa, at 950–1000°C at 4 GPa, at 1000–1050°C at 5 GPa, and <1000°C at 7 GPa for HPLC3, and at 950–1000°C at 3–5 GPa for HPLC4. The carbonate-out boundary was determined to be 950–1000°C at 3–5 GPa for both of HPLC3 and HPLC4, and <1000°C at 7 GPa for HPLC3. For HPLC3, experiments at 1050–1100°C showed carbonatite-silicate melt immiscibility with carbonate melt forming disconnected blobs in silicate melt matrix (Figure 2). Unlike in the alumina-rich carbonated bulk composition studied by *Thomsen and Schmidt* [2008], where kyanite was present at all conditions across the solidus, kyanite in our study only appeared at pressures and temperatures greater than 5 GPa and 1000°C (Table 1).

4. Discussion

4.1. The Effect of Water and Bulk Composition on Carbonated Pelite Melting

[8] Our experiments demonstrate that the fluid-absent, hydrous silicate solidus and phengite-out boundary of carbonated pelite at 3 GPa are lowered by ~50°C and ~100°C in the presence of excess fluid. This is owing to lower temperature of eutectic-type and peritectic-type melting for the solidus and phengite-breakdown, respectively in the H_2O vapor–pelite system (see details in *Tsuno and Dasgupta* [2012]). Although at 3 GPa carbonate-out temperatures are similar for the two bulk compositions, $calcite_{ss}$ mass fraction for HPLC3 between 900 and 950°C is distinctly lower than that of HPLC4 owing to the effect of excess-fluid in enhancing decarbonation for the former.

[9] At 5 GPa, however, the excess fluid has a limited influence on the solidus location, because the near-solidus melt is carbonatitic and thus has low activity of water. Consequently, both the solidus and carbonate-out boundary are similar for HPLC3 and HPLC4 and have the melting reactions across the solidus and carbonate-out boundary as follows:

$$0.5\ \text{cpx} + 0.5\ \text{phengite} + 3.1\ \text{calcite}_{ss} = 2.6\ \text{garnet} + 0.5\ \text{coesite} + 1.0\ \text{cbL}\ (\text{HPLC3};\ 900\text{–}950^\circ\text{C}) \quad (1)$$

$$0.9\ \text{cpx} + 2.6\ \text{K-feldspar} + 0.8\ \text{phengite} + 3.0\ \text{calcite}_{ss} = 3.6\ \text{garnet} + 2.7\ \text{coesite} + 1.0\ \text{cbL}\ (\text{HPLC4};\ 900\text{–}950^\circ\text{C}) \quad (2)$$

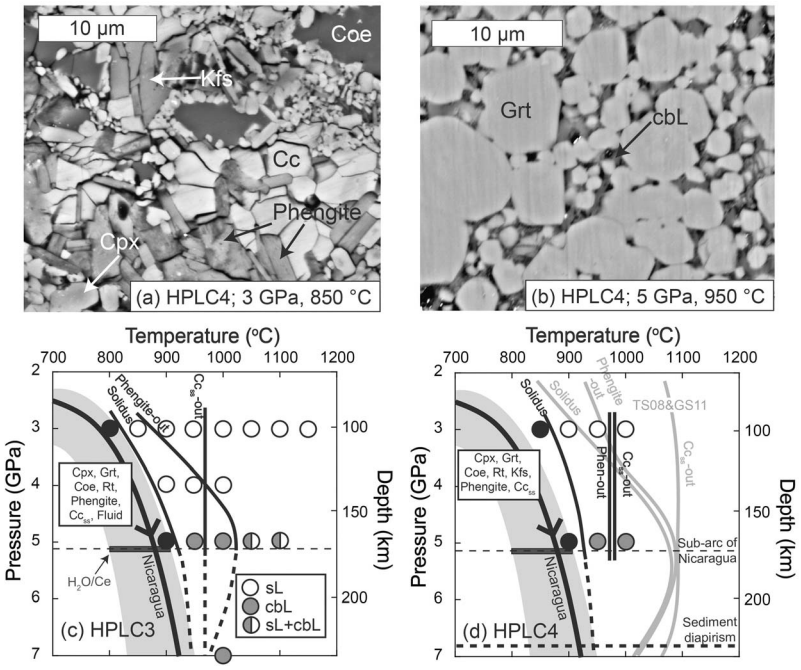

Figure 1. (a, b) Back-scattered electron images of run products. (a) A subsolidus experiment showing an assemblage of cpx, coesite, phengite, Fe-Mg calcite, and K-feldspar indicating the absence of fluid phase. Garnet and rutile are also present in this experiment but not present in the field of view shown here. (b) An experiment above the solidus, showing the presence of near solidus carbonatitic melt in residual garnet matrix. (c, d) Experimental phase relations of carbonated pelite from this study. (c) Minor fluid-present composition HPLC3 and (d) fluid-absent composition HPLC4. Subsolidus assemblages are shown in the boxed regions. The subsolidus conditions are shown in filled black symbols, and the conditions for the experiments with partial melts are shown in open circles (silicate melt), filled grey circles (carbonatite melt), and half filled circles (silicate-carbonate immiscible melts). Phase abbreviations are shown in Table 1. Also shown for comparison are the Nicaraguan slab-top trajectory (black line with arrow – geodynamic model prediction [*Syracuse et al.*, 2010] and gray-shaded region – geochemical prediction based on H_2O/Ce ratio [*Cooper et al.*, 2012]), sub-arc depth for Nicaragua subduction zone [*Syracuse et al.*, 2010], the predicted depth of initiation of sediment diapir under Nicaragua [*Behn et al.*, 2011], and the solidi, and phengite-out and calcite$_{ss}$-out boundaries for an alumina-rich, Fe-calcareous clay under minor-fluid present condition determined by *Thomsen and Schmidt* [2008] (2.5–5.0 GPa) and *Grassi and Schmidt* [2011a, 2011b] (≥5.5 GPa) (d).

$$1.09\ \text{cpx} + 0.19\ \text{phengite} + 1.85\ \text{calcite}_{ss} = 1.55\ \text{garnet} + 0.58\ \text{coesite} + 0.04\ \text{kyanite} + 1.0\ \text{cbL}\ (\text{HPLC3};\ 900\text{–}1000^{\circ}\text{C}) \quad (3)$$

$$1.1\ \text{cpx} + 0.6\ \text{K-feldspar} + 1.3\ \text{phengite} + 1.2\ \text{calcite}_{ss} = 0.8\ \text{garnet} + 1.4\ \text{coesite} + 1.0\ \text{kyanite} + 1.0\ \text{cbL}\ (\text{HPLC4};\ 900\text{–}1000^{\circ}\text{C}) \quad (4)$$

where equations (1) and (2) are solidus melting reactions and equations (3) and (4) are carbonate-out reactions relative to subsolidus conditions. These melting reactions indicate that in addition to calcite$_{ss}$ and phengite, cpx and K-feldspar are also key reactant phases to generate carbonate melt.

4.2. The Effect of Carbonated Pelite Bulk Composition on Near-Solidus Carbonate Melting and Decarbonation

[10] Comparison of our experiments with those by *Thomsen and Schmidt* [2008] (≤5 GPa) and *Grassi and Schmidt* [2011a, 2011b] (≥5.5 GPa) on an alumina-rich, carbonated pelite bulk composition (Figures 1c and 1d) highlights the importance of bulk composition on carbonated solidus. Compared to these published studies, the loci of carbonatite solidus, phengite-out, and carbonate-out boundaries of HPLC3 and HPLC4 at 5.0–5.5 GPa are ∼150°C, ∼50–100°C, and ∼100°C lower and these shifts in melting reactions arise because of different alumina content of the pelites (Table S1 in Text S1). Carbonate melt stability at much lower temperature at ∼5 GPa in our study results from significant contribution of cpx as a reactant phase in the melting reaction (equations 1–4), causing the release Na_2O to aid stability of alkali-rich melt at lower temperatures. The carbonate-forming melting reactions for our low-alumina pelites are in contrast with similar reaction of high-alumina pelite at similar pressures. At 5 GPa, the carbonate melt-forming melting reaction from the study of *Thomsen and Schmidt* [2008] can be expressed as

$$0.2\ \text{cpx} + 2.9\ \text{phengite} + 1.1\ \text{coesite} + 1.1\ \text{calcite}_{ss} = 0.7\ \text{grt} + 0.1\ \text{kyanite} + 3.3\ \text{sL} + 1.0\ \text{cbL}\ (5\ \text{GPa};\ \text{between}\ 1050\ \text{and}\ 1100^{\circ}\text{C}) \quad (5)$$

where much lower contribution of cpx in the production of carbonate melt is evident. High-alumina bulk compositions yield cpx with higher Jadeite ($NaAlSi_3O_8$) and Ca-tschermak ($CaAlAlSiO_6$) component at a given pressure and temperature (Figure S1 in Text S1), resulting in higher $D_{Na}^{cpx/carbonatite}$

Table 1. Summary of the Partial Melting Experiments on Hydrous, Carbonated Pelite[a]

Run Number	P (GPa)	T (°C)	t (h)	Mass Proportion (wt.%)											
				Cpx	Grt	Coe	Rt	Kfs	Kyanite	Phengite	Cc_{ss}	sL	cbL	Fluid	Sum r^2
HPLC3 (pelite + 1 wt.% H_2O + 5wt.% CO_2)															
G118-3	3	800	238	25.4 ± 3.9	20.7 ± 2.6	20.2 ± 1.3	0.4 ± 0.3	-	-	22.9 ± 2.4	10.3 ± 0.6	-	-	○	0.59
G112-3	3	850	249	27.7 ± 3.8	25.2 ± 0.9	16.1 ± 2.7	0.4 ± 0.2	tr.	-	17.1 ± 1.7	3.2 ± 0.4	10.4 ± 5.0		○	0.24
G120-3	3	900	234	26.2 ± 1.5	29.4 ± 0.4	2.5 ± 0.7	0.3 ± 0.3	tr.	-	-	0.6 ± 0.1	40.9 ± 0.7	-	○	0.24
G119-3	3	950	194	25.2 ± 4.5	28.5 ± 3.9	2.0 ± 3.6	0.4 ± 0.1	6.5 ± 4.7	-	-	0.2 ± 2.9	37.7 ± 5.5	-	○	1.00
G116-3	3	1000	160	21.2 ± 4.1	33.7 ± 5.4	3.2 ± 3.6	0.5 ± 0.2	-	-	-	-	41.5 ± 4.1	-	○	0.46
G106-3	3	1050	120	23.2 ± 1.5	30.8 ± 1.7	4.2 ± 0.5	0.3 ± 0.2	-	-	-	-	41.5 ± 0.5	-	○	0.47
G115-3	3	1100	69	24.3 ± 4.6	30.6 ± 5.7	2.7 ± 4.1	-	-	-	-	-	42.4 ± 4.8	-	○	0.60
G113-3	3	1150	53	27.6 ± 2.8	26.6 ± 2.5	4.4 ± 1.7	-	-	-	-	-	41.4 ± 1.4	-	○	0.61
BJJB186	4	900	93	17.9 ± 2.1	40.4 ± 2.6	20.7 ± 0.5	0.2 ± 0.1	-	-	11.5 ± 1.4	2.7 ± 0.3	6.6 ± 2.7	-	○	1.07
BJJB185	4	950	96	22.9 ± 1.7	40.4 ± 2.4	17.0 ± 3.4	0.3 ± 0.1	-	-	4.8 ± 4.5	1.2 ± 1.0	13.4 ± 5.4	-	○	0.12
BJJB188	4	1000	72	24.1 ± 0.9	37.7 ± 0.8	14.5 ± 1.9	-	-	-	-	-	23.7 ± 3.5	-	○	0.69
BJJB156	5	900	168	17.7 ± 2.5	33.0 ± 1.1	22.4 ± 1.1	0.2 ± 0.1	-	-	16.9 ± 2.1	9.8 ± 0.2	-	-	○	1.97
BJJB176	5	950	96	16.3 ± 5.7	39.8 ± 5.3	23.7 ± 1.7	0.3 ± 0.1	-	-	15.6 ± 4.6	1.7 ± 1.8	-	2.6 ± 2.2	-	0.23
BJJB155	5	1000	96	11.8 ± 1.6	41.2 ± 1.1	25.5 ± 1.3	0.1 ± 0.2	-	0.2 ± 1.2	15.9 ± 1.5	-	-	5.3 ± 1.3	-	0.02
BJJB178	5	1050	96	21.6 ± 1.2	39.8 ± 1.0	19.2 ± 0.8	-	-	2.0 ± 0.3	-	-	17.6 ± 0.7	0.1 ± 0.3	-	0.10
BJJB157	5	1100	72	25.0 ± 1.9	39.4 ± 1.1	20.1 ± 1.1	-	-	0.0 ± 0.0	-	-	15.5 ± 3.2	0.0 ± 1.4	-	0.46
BJJB177	7	1000	96	31.0 ± 0.3	40.4 ± 0.3	23.9 ± 0.2	-	-	0.0 ± 0.1	-	-	-	4.7 ± 0.2	-	2.63
HPLC4 (pelite + 0.5 wt.% H_2O + 5wt.% CO_2)															
B122	3	850	118	17.4 ± 2.5	23.2 ± 2.8	17.7 ± 2.2	0.5 ± 0.2	18.2 ± 4.5	-	12.0 ± 4.5	10.5 ± 0.6	-	-	-	1.29
B121[b]	3	900	77	(15.1 ± 3.6)	(28.3 ± 5.0)	(16.1 ± 4.5)	(0.5 ± 0.4)	(12.5 ± 4.0)	-	(8.5 ± 5.1)	(6.7 ± 3.0)	(11.3 ± 2.7)	-	-	-
B123	3	950	116	24.6 ± 2.4	27.5 ± 1.6	9.5 ± 1.5	0.4 ± 0.1	4.3 ± 0.8	-	7.4 ± 1.2	2.5 ± 0.4	23.8 ± 3.3	-	○	1.69
B132	3	1000	84	26.8 ± 4.4	29.7 ± 4.1	5.3 ± 3.2	0.1 ± 0.3	tr.	-	-	-	38.0 ± 5.4	-	○	0.94
BJJB198	5	900	119	20.2 ± 0.7	31.0 ± 1.9	20.7 ± 1.0	0.5 ± 0.2	5.5 ± 0.4	-	11.3 ± 1.0	10.7 ± 0.2	-	-	-	1.29
BJJB194[b]	5	950	120	(18.4 ± 5.8)	(38.6 ± 6.3)	(26.4 ± 5.6)	(0.5 ± 0.2)	-	-	(9.7 ± 4.5)	(4.3 ± 2.2)	-	(2.1 ± 1.1)	-	-
BJJB193	5	1000	72	10.7 ± 4.7	38.0 ± 2.8	33.1 ± 3.1	0.7 ± 0.2	-	8.5 ± 1.4	-	-	-	8.9 ± 0.9	-	0.99

[a]Cpx-clinopyroxene, Grt-garnet, Coe-coesite, Rt-rutile, Kfs - K-feldspar, Cc_{ss}-calcite solid solution, sL-hydrous silicate melt, and cbL-carbonate melt. Mass fractions of oxide phases are calculated by mass balance from compositions of the phases and of the starting mix: The errors are 1σ standard deviations using uncertainties of analyzed phase compositions. Note that Na_2O is not included for mass balance calculation except for subsolidus runs, owing to the Na-loss of sL and cbL analyzed by electron microprobe. 'Sum r^2' is the sum of oxide residuals square calculated based on bulk starting compositions, mineral modes, and phase composition and is a measure of convergence of the mass balance calculations.

[b]Based on the visual estimates assuming that the area of each phase in all experiments are proportional to the calculated mass fractions.

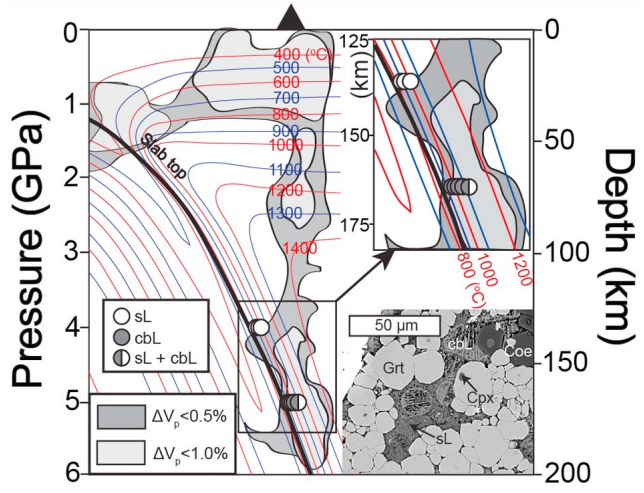

Figure 2. Thermal structure (blue and red curves) [*Peacock et al.*, 2005] and P-wave velocity perturbation (grey regions) [*Dinc et al.*, 2011] in the Nicaraguan subduction zone compared to the stability of fields of carbonate melt, immiscible carbonate and silicate melts, and silicate melts from our experiments. The deep low-velocity anomaly just above the slab coincides with the condition of carbonate melt generation and carbonate-silicate melt immiscibility. The inset presents a back-scattered electron image of one of our experiments showing the immiscible melts coexisting with cpx, coesite, and garnet (BJJB157; 5 GPa, 1100°C). Phase abbreviations are same as in Table 1.

and therefore higher bulk partition coefficient for Na, $D_{Na}^{pelite/carbonatite}$. In contrast, low-alumina HPLC3 and HPLC4 produce cpx with lower aluminous components (Table S2 and Figure S1 in Text S1), which result in lower $D_{Na}^{cpx/carbonatite}$ and thus lower $D_{Na}^{pelite/carbonatite}$ necessary for the stability of a more alkali-rich carbonatite at a lower temperature (Figure S2 in Text S1). Our study thus suggests that unlike the melting behavior of higher-alumina carbonated pelite, higher pressure melting of low-alumina compositions produce carbonatite flux at lower temperatures. Thus deep melting of subducted sediment results in a slab melt flux that is low in H_2O/CO_2 and with increasing temperature; carbonate-bound CO_2 release precedes phengite-bound H_2O release (Figure 3).

4.3. Deep Melting of Carbonated Sediment in the Nicaragua Subduction Zone

[11] Here we focus on subduction of carbonate-bearing sediments in the Central America subduction zone because the ocean-floor sediment drilled in Cocos plate contains carbonate [*Plank and Langmuir*, 1998]. Comparison of the solidi of HPLC3 and HPLC4 up to 5 GPa (~165 km depth) with top-slab depth-temperature trajectory of Nicaragua [*Syracuse et al.*, 2010] indicates that the sediment melting likely does not occur up to ~165 km depth (Figures 1c and 1d). However, extrapolation of the solidi and calcite-out boundaries as a function of depth suggests that carbonate melting of fluid-absent or fluid-poor sediment compositions can occur at depths as shallow as ~220–250 km (Figures 1c and 1d). This would especially be true if bend over of the solidus and carbonate-out boundary occur at greater depths (Figures 1c and 1d) as observed for aluminum-rich compositions [*Thomsen and Schmidt*, 2008; *Grassi and Schmidt*, 2011a, 2011b]. Alternatively, carbonate melting in the Central American subduction zones may also occur via diapiric rise of subducted sediments at a depth of ~230 km [*Behn et al.*, 2011]. This predicted depth of sediment melting is somewhat deeper than the proposed sub-arc depth of ~170 km [*Syracuse et al.*, 2010]. The experimental demonstration of deep carbonate melt generation at or near the slab-top conditions as presented here have both geophysical and geochemical implications.

4.4. Carbonate Melt Flux From Deeply Subducted Sediments: Cycling of CO_2 in the Sub-arc Mantle of Nicaragua

[12] Subduction of sedimentary carbonates is a key feature of Central American subduction zone [*Plank and Langmuir*, 1998] and primary arc magma from Nicaraguan arc volcanoes in particular show evidence of high CO_2 flux [e.g., *Roggensack et al.*, 1997; *Roggensack*, 2001; *Wehrmann et al.*, 2011]. Furthermore, other major (low SiO_2, Na_2O, and K_2O, high CaO, FeO) and trace element (e.g., high Ba/La, Sr/Ce) characteristics of Nicaraguan volcanoes [*Carr et al.*, 2003; *Sadofsky et al.*, 2008] compared to others along the arc suggest that the magma source characteristics of the former are different and may be explained by input from a carbonate melt [*Dasgupta et al.*, 2007a]. However, to date no clear mechanisms have been found that explains transfer of subducting carbonates to sub-arc mantle of Nicaragua. Firstly, the fate of carbonate bearing sediment compositions

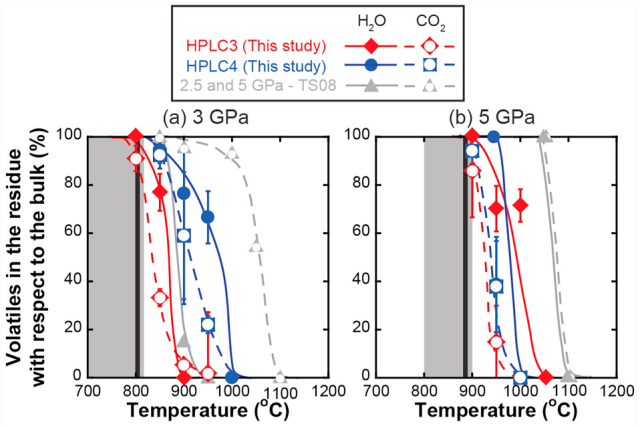

Figure 3. Relative fraction (in wt.%) of CO_2 and H_2O (solid symbols and lines for H_2O; symbols with white circles and broken lines for CO_2) retained in the residue at (a) 3 GPa and (b) 5 GPa. The sediment bulk compositions are HPLC3 (diamonds) and HPLC4 (circles) from this study and Al_2O_3-rich, Fe-calcareous clay from the study of *Thomsen and Schmidt* [2008] (triangles; TS08). Also shown are the present-day slab-top temperatures for Nicaragua at 3 and 5 GPa based on geodynamic modeling [*Syracuse et al.*, 2010] (black vertical lines) and geochemical constraints [*Cooper et al.*, 2012] (grey shaded box). The plots show that for low-Al pelites and at greater depths the breakdown of carbonate precedes the breakdown of phengite, generating a low H_2O/CO_2 fluid – a flux not generated during low-P hydrous melting and/or for high-Al pelite compositions at slab-top conditions.

relevant for the Central American subduction has been studied only to 3 GPa, i.e., conditions much shallower than the estimated depth of ~170 km [*Syracuse et al.*, 2010] to the top of the slab beneath volcanic front of Nicaragua. Secondly, the available experiments suggest that at conditions similar to that of the slab-top, breakdown of carbonate is limited and near-solidus melting produces a hydrous melt or fluid flux poor in carbon [*Kerrick and Connolly*, 2001a, 2001b; *Tsuno and Dasgupta*, 2012]. The data from this study shows that the scenario changes at higher pressures. At ≥5 GPa, the near-solidus melting produces Na and K-rich carbonatitic melt and phengite remains stable to relatively higher temperatures (Figure 3). Thus at depths in excess of 150 km, i.e., at sub-arc depth and beyond, the mantle wedge of Nicaragua likely receives a carbonatitic melt flux either by diapiric rise of carbonate-hemipelagic sediment mélange zone or by carbonate melting at slab-top conditions. A flux of sediment-derived carbonatite coming from these depths will metasomatize the shallower peridotitic mantle wedge, providing a source of CO_2 and thus causing a greater extent of melting than can be induced by hydrous flux alone [*Dasgupta et al.*, 2007b]. We propose that partial melting of sub-arc mantle wedge fluxed by carbonate melt along with hydrous flux (melt or fluid) can explain the elevated Ba/La, Sr/Ce and high CaO and lower SiO_2 of primary melt inclusions from Nicaraguan volcanic arcs [*Sadofsky et al.*, 2008]. Such flux of deep carbonated melt can also explain the higher flux of primary CO_2.

4.5. Evidence of Sediment Melt in Geophysical Properties of Nicaragua Mantle Wedge

[13] Our data of carbonate melting from deeply subducted sediments can also explain the signature of the negative V_P perturbation and high seismic attenuation that extend down to 200 km below the volcanic front in Nicaragua [*Dinc et al.*, 2011; *Syracuse et al.*, 2008] (also see Figure 2). We argue that the low seismic wave speeds and high attenuation may be explained by impregnation of carbonatitic melt coming from ~230–260 km deep slab. One question, however, is the dynamic stability of carbonated melt at these depths because carbonatite is expected to be extremely mobile in the mantle based on the measurements of density and viscosity [*Dobson et al.*, 1996], dihedral angle [*Minarik and Watson*, 1995] and infiltration distance [*Hammouda and Laporte*, 2000] in silicate mineral matrix. We suggest, based on our textural observation of carbonate melt-silicate melt immiscibility, that entrapment of isolated carbonate melt pockets in viscous silicate melt may cause temporary retention of carbonate melt just above the deep sub-arc depth of Nicaragua. In Figure 2 we show the silicate/carbonatite melt stability for carbonated pelite bulk compositions studied here in the framework of thermal structure of the Nicaragua subduction zones [*Peacock et al.*, 2005]. It can be observed that the field of silicate-carbonatite melt immiscibility is indeed located right above the slab at ~165 km depth and it also coincides with the low V_p region mapped by *Dinc et al.* [2011]. Because the generation of silicate partial melts of sedimentary protolith requires temperatures ≥1050°C at >150 km, immiscibility-induced trapping of carbonate melt requires sedimentary parcel being subjected to higher temperatures than what can be experienced along the *P-T* path of subduction in Nicaragua. Thus once again, diapiric rise of sediment parcel from ≥200 km depth may be the cause of generating less mobile silicate melt, which in turn traps carbonatitic melt coming from greater depths. The numerical calculations of *Gorczyk et al.* [2006] and *Behn et al.* [2011] also support such possibility, as these authors suggest that upwelling of sediment parcel for young subducted slab such as Nicaragua happens from relatively deep upper mantle conditions at ≥230 km.

[14] **Acknowledgments.** We thank Anne Peslier and Kent Ross for help with the electron microbe analyses and greatly appreciate thoughtful comments by two anonymous reviewers. This work was supported by NSF grant OCE-0841035 to R. D.

[15] The Editor thanks two anonymous reviewers for their assistance evaluating this paper.

References

Behn, M. D., P. B. Kelemen, G. Hirth, B. R. Hacker, and H.-J. Massonne (2011), Diapirs as the source of the sediment signature in arc lavas, *Nat. Geosci.*, *4*, 641–646, doi:10.1038/ngeo1214.

Carr, M. J., M. D. Feigenson, L. C. Patino, and J. A. Walker (2003), Volcanism and geochemistry in Central America: Progress and problems, in *Inside the Subduction Factory*, *Geophys. Monogr. Ser.*, vol. 138, edited by J. Eiler, pp. 153–174, AGU, Washington, D. C.

Cooper, L. B., D. M. Ruscitto, T. Plank, P. J. Wallace, E. M. Syracuse, and C. E. Manning (2012), Global variations in H_2O/Ce: 1. Slab surface temperatures beneath volcanic arcs, *Geochem. Geophys. Geosyst.*, *13*, Q03024, doi:10.1029/2011GC003902.

Dasgupta, R., and M. M. Hirschmann (2010), The deep carbon cycle and melting in Earth's interior, *Earth Planet. Sci. Lett.*, *298*, 1–13, doi:10.1016/j.epsl.2010.06.039.

Dasgupta, R., M. M. Hirschmann, and A. C. Withers (2004), Deep global cycling of carbon constrained by the solidus of anhydrous, carbonated eclogite under upper mantle conditions, *Earth Planet. Sci. Lett.*, *227*, 73–85, doi:10.1016/j.epsl.2004.08.004.

Dasgupta, R., M. M. Hirschmann, and N. Dellas (2005), The effect of bulk composition on the solidus of carbonated eclogite from partial melting experiments at 3 GPa, *Contrib. Mineral. Petrol.*, *149*, 288–305, doi:10.1007/s00410-004-0649-0.

Dasgupta, R., M. M. Hirschmann, and N. D. Smith (2007a), Partial melting experiments of peridotite + CO_2 at 3 GPa and genesis of alkalic ocean island basalts, *J. Petrol.*, *48*, 2093–2124, doi:10.1093/petrology/egm053.

Dasgupta, R., M. M. Hirschmann, and N. D. Smith (2007b), Water follows carbon: CO_2 incites deep silicate melting and dehydration beneath mid-ocean ridges, *Geology*, *35*, 135–138, doi:10.1130/G22856A.1.

de Leeuw, G. A. M., D. R. Hilton, T. P. Fischer, and J. A. Walker (2007), The He-CO_2 isotope and relative abundance characteristics of geothermal fluids in El Salvador and Honduras: New constraints on volatile mass balance of the Central American volcanic arc, *Earth Planet. Sci. Lett.*, *258*, 132–146, doi:10.1016/j.epsl.2007.03.028.

Dinc, A. N., W. Rabbel, E. R. Flueh, and W. Taylor (2011), Mantle wedge hydration in Nicaragua from local earthquake tomography, *Geophys. J. Int.*, *186*, 99–112, doi:10.1111/j.1365-246X.2011.05041.x.

Dobson, D. P., A. P. Jones, R. Rabe, T. Sekine, K. Kurita, T. Taniguchi, T. Kondo, T. Kato, O. Shimomura, and S. Urakawa (1996), In-situ measurement of viscosity and density of carbonate melts at high pressure, *Earth Planet. Sci. Lett.*, *143*, 207–215, doi:10.1016/0012-821X(96)00139-2.

Gerbode, C., and R. Dasgupta (2010), Carbonate-fluxed melting of MORB-like pyroxenite at 2.9 GPa and genesis of HIMU ocean island basalts, *J. Petrol.*, *51*, 2067–2088, doi:10.1093/petrology/egq049.

Gorczyk, W., T. V. Gerya, J. A. D. Connolly, D. A. Yuen, and M. Rudolph (2006), Large-scale rigid-body rotation in the mantle wedge and its implications for seismic tomography, *Geochem. Geophys. Geosyst.*, *7*, Q05018, doi:10.1029/2005GC001075.

Grassi, D., and M. W. Schmidt (2011a), The melting of carbonated pelites from 70 to 700 km depth, *J. Petrol.*, *52*, 765–789, doi:10.1093/petrology/egr002.

Grassi, D., and M. W. Schmidt (2011b), Melting of carbonated pelites at 8–13 GPa: Generating K-rich carbonatites for mantle metasomatism, *Contrib. Mineral. Petrol.*, *162*, 169–191, doi:10.1007/s00410-010-0589-9.

Green, T. H., and P. L. Hellman (1982), Fe-Mg partitioning between coexisting garnet and phengite at high pressure, and comments on a garnet-phengite geothermometer, *Lithos*, *15*, 253–266, doi:10.1016/0024-4937(82)90017-2.

Hammouda, T., and D. Laporte (2000), Ultrafast mantle impregnation by carbonatite melts, *Geology*, *28*, 283–285, doi:10.1130/0091-7613(2000)28<283:UMIBCM>2.0.CO;2.

Kerrick, D. M., and J. A. D. Connolly (2001a), Metamorphic devolatilization of subducted marine sediments and the transport of volatiles into the Earth's mantle, *Nature*, *411*, 293–296, doi:10.1038/35077056.

Kerrick, D. M., and J. A. D. Connolly (2001b), Metamorphic devolatilization of subducted oceanic metabasalts: Implications for seismicity, arc magmatism and volatile recycling, *Earth Planet. Sci. Lett.*, *189*, 19–29, doi:10.1016/S0012-821X(01)00347-8.

Kiseeva, E. S., G. M. Yaxley, J. Hermann, K. D. Litasov, A. Rosenthal, and V. S. Kamenetsky (2012), An experimental study of carbonated eclogite at 3.5–5.5 GPa: Implications for silicate and carbonatemetasomatism in the cratonic mantle, *J. Petrol.*, *53*, 727–759, doi:10.1093/petrology/egr078.

Krogh Ravna, E. (2000), The garnet-clinopyroxene Fe^{2+}-Mg geothermometer: An updated calibration, *J. Metamorph. Geol.*, *18*, 211–219, doi:10.1046/j.1525-1314.2000.00247.x.

Minarik, W. G., and E. B. Watson (1995), Interconnectivity of carbonate melt at low melt fraction, *Earth Planet. Sci. Lett.*, *133*, 423–437, doi:10.1016/0012-821X(95)00085-Q.

Peacock, S. M., P. E. van Keken, S. D. Holloway, B. R. Hacker, G. A. Abers, and R. L. Fergason (2005), Thermal structure of the Costa Rica–Nicaragua subduction zone, *Phys. Earth Planet. Inter.*, *149*, 187–200, doi:10.1016/j.pepi.2004.08.030.

Plank, T., and C. H. Langmuir (1998), The chemical composition of subducting sediment and its consequences for the crust and mantle, *Chem. Geol.*, *145*, 325–394, doi:10.1016/S0009-2541(97)00150-2.

Roggensack, K. (2001), Sizing up crystals and their melt inclusions: a new approach to crystallization studies, *Earth Planet. Sci. Lett.*, *187*, 221–237, doi:10.1016/S0012-821X(01)00269-2.

Roggensack, K., R. L. Hervig, S. B. McKnight, and S. N. Williams (1997), Explosive basaltic volcanism from Cerro Negro volcano: Influence of volatiles on eruptive style, *Science*, *277*, 1639–1642, doi:10.1126/science.277.5332.1639.

Sadofsky, S. J., M. Portnyagin, K. Hoernle, and P. van den Bogaard (2008), Subduction cycling of volatiles and trace elements through the Central American volcanic arc: Evidence from melt inclusions, *Contrib. Mineral. Petrol.*, *155*, 433–456, doi:10.1007/s00410-007-0251-3.

Shaw, A. M., D. R. Hilton, T. P. Fischer, J. A. Walker, and G. E. Alvarado (2003), Contrasting He-C relationships in Nicaragua and Costa Rica: Insights into C cycling through subduction zones, *Earth Planet. Sci. Lett.*, *214*, 499–513, doi:10.1016/S0012-821X(03)00401-1.

Snyder, G., R. Poreda, A. Hunt, and U. Fehn (2001), Regional variations in volatile composition: Isotopic evidence for carbonate recycling in the Central American volcanic arc, *Geochem. Geophys. Geosyst.*, *2*(10), 1057, doi:10.1029/2001GC000163.

Syracuse, E. M., G. A. Abers, K. Fischer, L. MacKenzie, C. Rychert, M. Protti, V. González, and W. Strauch (2008), Seismic tomography and earthquake locations in the Nicaraguan and Costa Rican upper mantle, *Geochem. Geophys. Geosyst.*, *9*, Q07S08, doi:10.1029/2008GC001963.

Syracuse, E. M., P. E. van Keken, G. A. Abers, D. Suetsugu, C. Bina, T. Inoue, D. Wiens, and M. Jellinek (2010), The global range of subduction zone thermal models, *Phys. Earth Planet. Inter.*, *183*, 73–90, doi:10.1016/j.pepi.2010.02.004.

Thomsen, T. B., and M. W. Schmidt (2008), Melting of carbonated pelites at 2.5–5.0 GPa, silicate-carbonatite liquid immiscibility, and potassium-carbon metasomatism of the mantle, *Earth Planet. Sci. Lett.*, *267*, 17–31, doi:10.1016/j.epsl.2007.11.027.

Tsuno, K., and R. Dasgupta (2011), Melting phase relation of nominally anhydrous, carbonated pelitic-eclogite at 2.5–3.0 GPa and deep cycling of sedimentary carbon, *Contrib. Mineral. Petrol.*, *161*, 743–763, doi:10.1007/s00410-010-0560-9.

Tsuno, K., and R. Dasgupta (2012), The effect of carbonates on near-solidus melting of pelite at 3 GPa: Relative efficiency of H_2O and CO_2 subduction, *Earth Planet. Sci. Lett.*, *319–320*, 185–196, doi:10.1016/j.epsl.2011.12.007.

van Keken, P. E., B. R. Hacker, E. M. Syracuse, and G. A. Abers (2011), Subduction factory: 4. Depth-dependent flux of H_2O from subducting slabs worldwide, *J. Geophys. Res.*, *116*, B01401, doi:10.1029/2010JB007922.

Wehrmann, H., K. Hoernle, M. Portnyagin, V. I. Vernadsky, M. Wiedenbeck, and K. Heydolph (2011), Volcanic CO_2 output at the Central American subduction zone inferred from melt inclusions in olivine crystals from mafic tephras, *Geochem. Geophys. Geosyst.*, *12*, Q06003, doi:10.1029/2010GC003412.

Yaxley, G. M., and G. P. Brey (2004), Phase relations of carbonate-bearing eclogite assemblages from 2.5 to 5.5 GPa: Implications for petrogenesis of carbonatites, *Contrib. Mineral. Petrol.*, *146*, 606–619, doi:10.1007/s00410-003-0517-3.